Flow field around bubbles on formation of air embolism in small vessels

Zhongnan Li[a,1] , Guiling Li[b,1] , Yongjian Li[c,2] , Yuexin Chen[d,2], Jiang Li (李疆)[e] , and Haosheng Chen (陈皓生)[a,2]

[a]State Key Laboratory of Tribology, Tsinghua University, 100084 Beijing, China; [b]School of Medicine, Tsinghua University, 100084 Beijing, China; [c]Department of Mechanical Engineering, Tsinghua University, 100084 Beijing, China; [d]Peking Union Medical College Hospital, Chinese Academy of Medical Sciences, 100730 Beijing, China; and [e]School of Mechanical Engineering, University of Science and Technology Beijing, 100083 Beijing, China

An air embolism is induced by intravascular bubbles that block the blood flow in vessels, which causes a high risk of pulmonary hypertension and myocardial and cerebral infarction. However, it is still unclear how a moving bubble is stopped in the blood flow to form an air embolism in small vessels. In this work, microfluidic experiments, in vivo and in vitro, are performed in small vessels, where bubbles are seen to deform and stop gradually in the flow. A clot is always found to originate at the tail of a moving bubble, which is attributed to the special flow field around the bubble. As the clot grows, it breaks the lubrication film between the bubble and the channel wall; thus, the friction force is increased to stop the bubble. This study illustrates the stopping process of elongated bubbles in small vessels and brings insight into the formation of air embolism.

air embolism | bubbles | microfluidics | thrombosis | blood flow

Air embolism is the entrapment of air bubbles into vascular structures (1, 2). It often happens in therapeutic procedures such as injection and surgeries (3, 4). It also occurs in diving or aerospace activities in which the environmental pressure changes rapidly (5). The air embolism often causes tissue ischemia and results in myocardial infarct or brain damages (6, 7). In clinical studies (8–10), it is common to find that a single bubble is trapped in a small vessel with diameter of the order of 100 μm to form an air embolism. However, it is still unknown how the bubble is brought to rest in small vessels and what the effect of the fluid dynamics on the stopping process is. The understanding of the fluid dynamics of a moving bubble confined in a small vessel will bring insight on the mechanism of the air embolism and is also crucial to the prevention and treatment of the air embolism.

The air embolism has been well studied when a bubble is trapped in a vessel and contacts the endothelial layer (11–13). However, it is still unclear how a bubble moving along with the continuous blood flow stops in the vessel. It is usually believed that the bubble is stopped by the friction force on it. However, according to Taylor and Bretherton's theory (14, 15), a bubble will become a Taylor bubble, which is deformed and elongated, when it flows in a smaller channel, and a thin lubrication film of the surrounding liquid will form around it. Therefore, the bubble will keep flowing without contacting the channel wall. The Laplace pressure from the bubble surface is considered another reason to stop the bubble. When a bubble encounters a junction of the vessel, the Laplace pressure caused by the deformation of surface at the head of the bubble may be able to overcome the blood pressure (16). However, when the radius of the vessel is equal to or greater than 100 μm, the Laplace pressure of the bubble is lower than 1 kPa, which is much less than the driving pressure, ~10 to 15 kPa, in the small arteries (17). In the other case, when a bubble is moving in a small vessel, the confined bubble surface results in higher pressure within the bubble, which will squeeze the lubrication film to build up drag resistance. However, it is also too low to stop the bubble. To reveal the dominant reason a bubble would stop in small vessels, the braking process of the

bubble needs to be observed and studied. However, it is still difficult to show the motion of a bubble and its surrounding flow fields in small vessels. The current methods, such as computed tomography, contrast-enhanced ultrasound, magnetic resonance images, and echocardiography (18–20), are not able to provide a high-resolution flow field around the moving bubble.

In this work, in vivo and in vitro experiments are performed to show the motion of a bubble during its braking process in the small vessels. Microfluidic devices are made to show the flow field around a moving bubble, and the effect of the flow field on the coagulation on the bubble surface is illustrated. During the coagulation, the variation of the lubrication film and the corresponding friction force on the bubble are both measured to explain the reason for the stopping of the bubble.

In Vivo Observation on Formation of Air Embolism Formation of an air embolism is observed in vivo in the mesenteric vascular network of a rabbit. Blood mixed with air bubbles is injected into mesenteric vascular vessels of the rabbit, and the motion of a bubble in a small vessel is then observed by a fluorescent microscope. The schematics of the experiment are shown in Fig. 1 A and B, and the experimental details are introduced in *Materials and Methods*.

Significance

Circulatory air embolisms resulting from surgical procedures or deep-sea diving can cause pathophysiological responses such as pulmonary hypertension and cardio-cerebral infarction. Despite significant research on embolism treatment, underlying processes of how moving bubbles get stuck in vessels have not been fully established. To further this mechanistic understanding, we developed microfluidic and in vivo experiments to observe bubble's stopping process and revealed that aggregation of blood cells and thrombus formation occurs on the periphery of embolism's tail because of flow recirculation. This localized thrombus formation triggers dramatic increase in flow resistance that stops bubble's motion. This study brings insight into the critical stage of air embolism formation and may lead to strategies for prevention and treatment of this clinically significant event.

In a vessel with the diameter of 200 μm, an injected bubble that reflects the red color is observed to flow through two junctions and finally stop in the vessel to form an air embolus, as shown by a
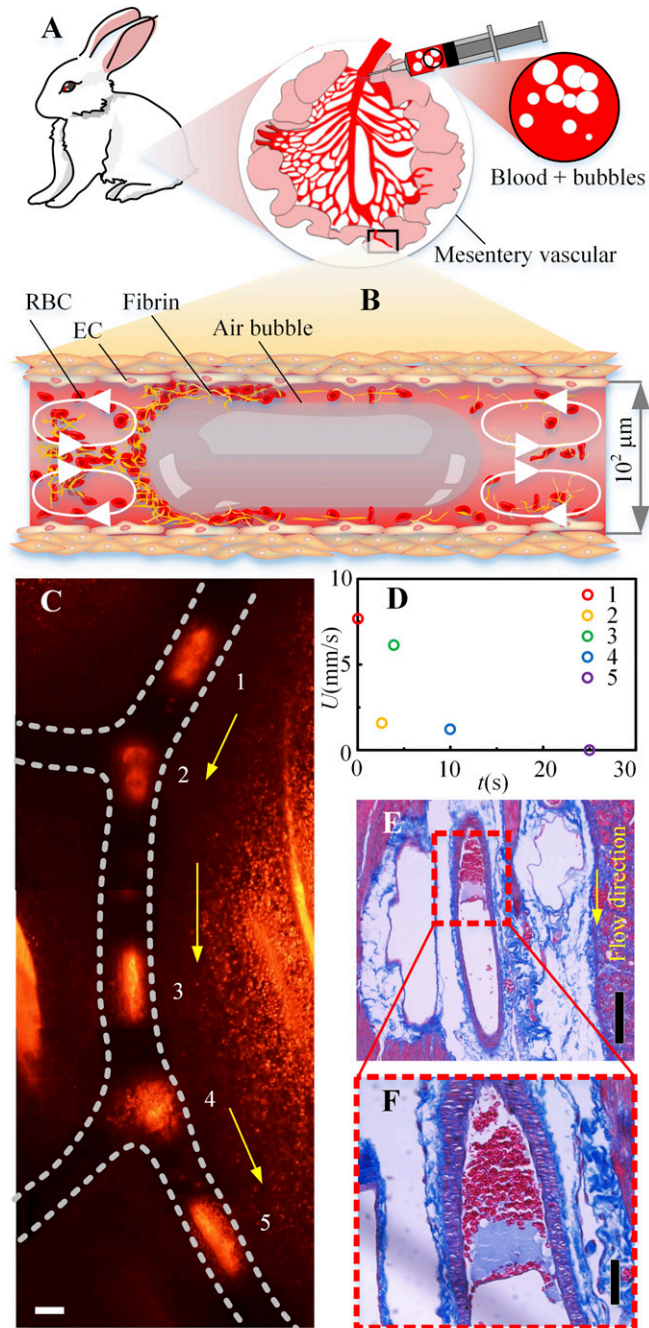

Fig. 1. In vivo experiment of air embolism formed in mesenteric vascular vessels of a rabbit. (*A*) Schematics of the in vivo experiment. (*B*) Schematics of the flow fields around a flowing bubble confined in a vessel and the aggregation of RBCs on the bubble surface. (*C*) The combined images of the stopping process of a bubble flowing in a small vessel in time series. The red color is the reflection of light from the bubble surface, which indicates the position of the bubble. The video of the moving bubble is provided in Movie S1. (*D*) The velocity of the bubble at the locations of 1 to 5 as marked in image *C*. (*E*) Masson-stained histological section of the air embolus taken from the vessel along the flow direction, and *F* is the clot formed at the tail of the bubble, corresponding to the location in the dashed box in *E*. (The scale bars in *C–F* are 100 μm.)

combined image of the time series of the moving bubble in Fig. 1*C*, where the bubble flows from location 1 to location 5 with variation in its shape. In addition, the velocities of the bubble at the five locations are shown in Fig. 1*D*. The in vivo experiment clearly shows that a bubble deforms into a Taylor bubble and flows as a slug flow in the small vessel (21), in which the bubble is squeezed to form a long bubble and followed by a segment of liquid. The bubble gradually comes to rest in the vessel. This result is different from the suggestion that an air embolism is caused by a spherical bubble as soon as it forms from the dissolved gas in blood (2), and the shape of the bubble observed in this experiment is consistent with the studies reported before (22–24). The dynamic observation provides the details about the process of how the Taylor bubble transports, deforms, and finally stops in the small vessel.

The air emboli formed in small vessels in vivo are taken out to be examined under a microscope. It is interesting to find that the clot is formed at the tail of the bubbles, as shown by the histological section of the air embolus in Fig. 1 *E* and *F*. The section is stained by Masson and red blood cells (RBCs), and the fibrin are found in the section of the clot. The clot formed at the tail illustrates that the coagulation happens unevenly on the bubble, and it indicates that the flow field around the bubble plays an important role. This finding has not been reported in previous studies including clinical anatomy (1–3) and rheological experiments (25, 26). In clinical anatomy, a thin layer consisted of cells and fibrins is also found on the bubble surface but it is observed on the cross-section of the vessel, and the uneven distribution of the clot on the bubble along the flowing direction is not seen. In rheological experiments (25, 26), the Couette flow is different from the slug flow for a Taylor bubble; thus, the clot is not formed at the tail of the bubble.

This finding raises another interesting question: Does the clot form to stop the bubble, or does the bubble stop to form the clot? Although the uneven distribution of the thrombus on the bubble indicates that the clot starts to form when the bubble is moving, it is still necessary to observe the coagulation on a bubble during its stopping process. Since it is difficult to observe the coagulation and the flow field in vessels, in vitro experiments are performed as follows.

In Vitro Experiments on an Air Embolism T-junction polydimethylsiloxane PDMS) microchannel is fabricated according to the soft photolithography method (27), and its cross-section and the size are shown in Fig. 2*A*. The inner surface of the channel is coated by bovine serum albumin (BSA) to avoid coagulation. The fibrinogens in the injected blood are dyed (*Materials and Methods*), which will emit red fluorescence when they are cross-linked into fibrin once the coagulation occurs. Blood and air are injected into the channel through separated inlets. At the junction of the channels, bubbles are formed with the size controlled by the flow rate ratio of the blood to the air. According to the observed bubble in the in vivo experiment, the bubble length in the channel is controlled to be ~3 to 5 times larger than the channel size. The flow velocity of the blood is 7.0 mm/s, which is in the order of 10 mm/s of the blood flow in arterioles with the diameter of 0.2 mm (28, 29).

Firstly, the formation of an air embolism is observed in the devices. In the transparent channel, the origin of a clot at the tail of an injected bubble can be seen clearly during the stopping process of the bubble, as shown in Fig. 2 *B* and *C*. When the bubble enters the channel, it elongates, and the flow becomes a slug flow. The coagulation does not happen on the bubble surface yet and there is no fluorescence around the bubble. As the bubble is flowing, fluorescence appears to indicate the formation of a clot at the tail of the bubble, as shown in Fig. 2*B*, and the speed of the bubble is found to decrease as shown in Fig. 2*D*. As the clot grows at the tail, it finally stops the motion of the bubble at the curved section of the channel, as shown in Fig. 2 *C* and *D*.

2 of 6 | PNAS
https://doi.org/10.1073/pnas.2025406118

Li et al.
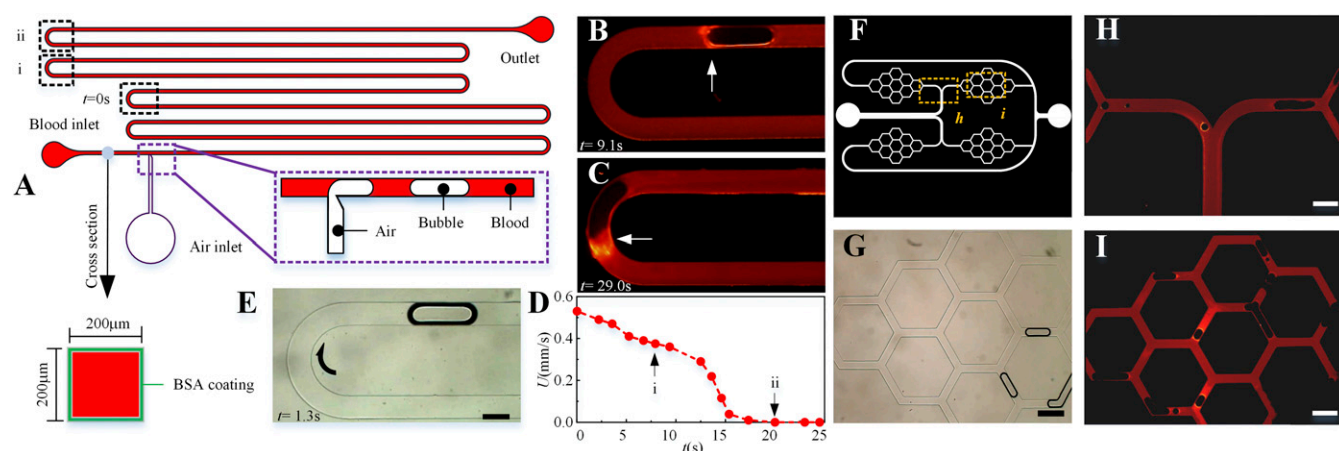Flow field around bubbles on formation of air embolism in small vessels

Fig. 2. In vitro experiments of the air embolism performed on microfluidic devices. (*A*) The cross-section of the channel is square, and it is coated with a BSA layer. (*B* and *C*) The origin and growth of the blood clot at the tail of a bubble at the different positions as marked in *A*. (*D*) The velocity of the bubble during its stopping process. (*E*) A bubble passes through the channel without stopping in glycerol solution. (*F*) A microfluidic vessel network with a four-level structure. (*G*) Bubbles pass through the network in glycerol solution. (*H* and *I*) Bubbles pass through the second to third levels but stop in the fourth level. (Scale bars, 200 μm.)

This experiment clarifies that the coagulation happens on the bubble surface when the bubble is still moving in the vessel, and the coagulation on the bubble affects the braking of the bubble. To validate the effect of the coagulation on the slowing down of the bubble, blood is replaced by glycerol water solution with the same viscosity (η ∼4 mPa · s), and bubbles are seen to flow through the channel rapidly without stopping, as shown in Fig. 2*E*. It validates that the coagulation on the bubble surface is a dominant factor during the formation of an air embolism in a small vessel.

Furthermore, a channel network is fabricated to simulate a more complex vascular network. The PDMS channel network has 4 levels with the sizes of 500, 240, 150, and 100 μm for each level, as shown in Fig. 2*F*. When the continuous phase is the glycerol solution, the bubbles are observed to flow through the network without stopping under the driven pressure of 10 kPa, as shown in Fig. 2*G*. The corresponding video is provided in Movie S2. However, when the blood is used, the bubbles stop in the fourth level and clots are found on their surface, as shown in Fig. 2 *H* and *I*, respectively. The video is provided in Movie S3.

In the in vitro experiments, the origination of the clot at the tail of the bubble is clearly illustrated by the fluorescence during the stopping process of the bubble in the channel, which repeats the same results with those found in the in vivo experiments. They also reveal the relationship between the coagulation on the bubble surface and the stopping of the bubble. It confirms that, in the slug flow, the coagulation is the dominant factor for the stopping of the bubble instead of the Laplace pressure.

Secondly, the flow field around the bubble is measured to explain why the clot originates at the tail of the bubble. The transparent microchannel makes it possible to measure the flow field around the bubble during its stopping process. To see the flow field more clearly, diluted blood with hematocrit (HCT) of 1% is used in the measurement. The motion of the RBCs around a flowing bubble is captured by a high-speed camera. The flow field is derived in Micro-Particle Image Velocimetry software (*Materials and Methods*).

At the tail of the bubble, there are a pair of recirculation zones of the blood flow, as shown in Fig. 3*A*. Near the bubble surface, most of the blood is flowing toward the bubble, which brings blood cells onto the bubble surface. In contrast, on the head of the bubble, there are also a pair of recirculation zones of the blood flow, but most of the blood is flowing away from the bubble, thus the cells are pushed away from the bubble surface. With respect to the bubble surface, the opposite-flowing direction of the blood explains why the clot is formed at the tail of a flowing bubble. The

measured flow field around the bubble is consistent with the fluidic model established in droplet microfluidics, as shown by the schematics in Fig. 3*B* (30). The mechanism has been studied by Stebe in the research of remobilizing the surfactant concentration at the bubble interface (31), and a similar flow field has been visualized by Yamaguchi using microparticle image velocimetry (32). On the bubble surface, there are six stagnant points (i)-(vi). That means that particles on the surface will be brought toward these points. Among them, points (iv) and (vi), which are part of a ring on the rear caps of the bubble, are kinematically stable points. Thus, the blood cells and fibrinogens driven by the flow will move toward the two points and aggregate there. To show the aggregation of particles on the bubble surface more clearly, larger poly methyl methacrylate particles with the size of 20 μm are used in the experiment. The microparticles are observed to aggregate at the points (iv) and (vi) at the tail of the bubble, as shown in Fig. 3*C*. The same effect can be seen in the experiments with RBCs and other sizes of particles, which are shown in *SI Appendix*, Fig. S2. The result confirms that the flow fields around the bubble carries blood cells and fibrinogens to the stagnant points, and the aggregation of the cells and fibrinogens at the points causes the formation of fibrins and the origination of clot at the tail of a moving bubble.

Under the influence of the flow field, the cell aggregation is observed to extend backward (opposite to the flow direction), as well as forward (along the flow direction), which is shown in Movie S4. The reason for the cell aggregation to grow backward is attributed to the flow field behind the bubble that keeps bringing cells to the tail of the bubble. The forward growth of the cell aggregation is attributed to the flow along the head-to-tail streamlines on the bubble surface, as shown in Fig. 3*B*, which brings cells from the head of the bubble. According to the lubrication theory by Bretherton (17), there is a lubrication film between the bubble and the wall, which provides a gap for the cells on the head to move to reach the tail of the bubble.

In the experiment, blood cells are seen to flow from the head to the tail on the bubble surface, as shown in Fig. 3*D*. However, the number of cells traveling in this way is quite low. This can be attributed to the Fåhræus-Lindqvist Effect (33), which causes a decrease of RBC concentration (hematocrit level) when the blood flows from the channel to the thin lubrication film. When the cells reach the tail of the bubble, they will be stopped by the cell aggregation already formed there; thus, the cell aggregation will extend forward through the gap between the bubble and the
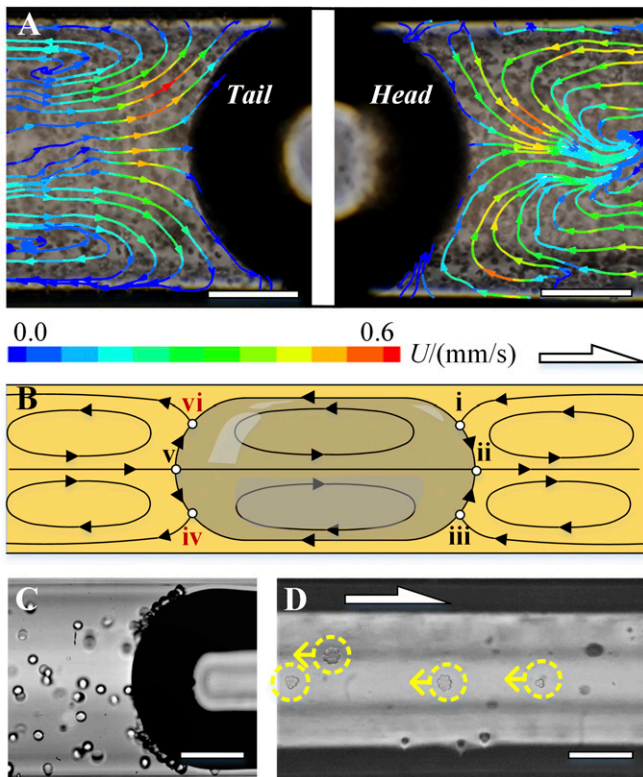
Fig. 3. Flow field around a moving bubble and the formation of the cell aggregation at the tail. (*A*) Measured flow fields around the tail and the head of the bubble. The black points on the background are the RBCs. (*B*) Schematics of the flow field around the bubble surface and the stagnant points on the bubble surface. (i) through (vi) are stagnant points, and only (iv) and (vi) are kinematically stable points. (*C*) Poly methyl methacrylate particles are seen to adhere on the stable stagnant points at the tail of a moving bubble. (*D*) Blood cells and fibrin (marked in the circles) are flowing in the lubrication film from the head to the tail of the bubble. (Scale bars, 100 μm.)

wall. It should be noted that the forward growth of the cell aggregation is much slower than the backward growth because most of the cells near the head of the bubble are flowing away from the bubble surface along the streamlines and only a few cells reaching the head of the bubble can flow to the tail along the head-to-tail streamlines.

The measured flow field around the bubble shows the aggregation of the blood cells. The aggregation points around the bubble are consistent with the locations where the fluorescent labeled fibrins appear. It reveals the close relation between the motion of blood cell driven by the flow and the formation of clot around the bubble. It explains why the clot originates at the tail of the bubble, and it clearly demonstrates that the fluid dynamics of the slug flow play a dominant role in the formation of air embolism.

Lubrication Film and Friction Force Measurement Along with the aggregation of blood cells and fibrinogens, the fibrins appear, and then the clot grows on the bubble surface. The clot occupies part of the space of the lubrication film around the bubble, and the friction force on the bubble increases to stop the bubble, as shown in Fig. 4*A*. The lubrication film around the bubble is measured during the growth of the clot using an interference method (34). The thickness of the lubrication film is calculated according to the interference fringes, as shown in Fig. 4 *B*, *i* and *ii*. The details on the measurement and the calculation are provided in *SI Appendix*. As the clot grows, a dark region appears at the tail of the interference fringes, as shown in Fig. 4*C*. It indicates that there is no

lubrication film in this region and the clot on the bubble contacts the wall of the channel. The length of the contacting region is evaluated by the contact length l_c.

The change of the friction force on the bubble is measured during the variation of the lubrication film using a push-stop method. A controlled pressure is applied at the inlet to push the bubble to move in the channel. When the bubble stops because of the growth of the clot on its surface, the pressure is increased until the bubble is pushed to move again. As soon as the bubble is moved by the increased pressure, the contact length of the bubble is recorded. The product of the increased pressure and the cross-sectional area of the channel equals to the maximum static friction force on the bubble. As the cross-sectional areas of channels are kept unchanged in these experiments, the increased pressure is directly used to represent the friction resistance to the motion of the bubble. Using this push-stop method, the friction resistances on the air emboli with the different contact length are obtained. They clearly show that the growth of the clot changes the lubrication status of the bubble. The increased friction force between the bubble and the channel will stop the bubble to cause air embolism in the channel.

Discussion

In this work, the flow field around a bubble is demonstrated to be a dominant factor to influence the formation of the air embolism in a small channel with the size of hundreds of microns. In fact, the vascular vessels have more complex structures, shapes, and sizes, which also influence the formation of air embolism.

Firstly, the size of the vessel is an important factor to affect the stopping of the bubble from its flowing status. Based on the
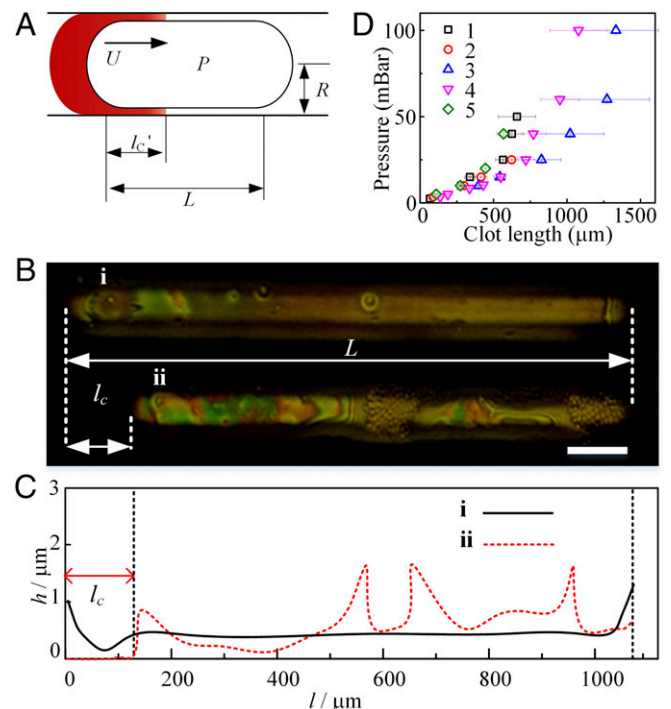

Fig. 4. The measured lubrication status and the friction force on the bubble. (*A*) Schematics of the lubrication status of a bubble changed by the clot on the bubble surface. (*B*, *i* and *ii*) The interference fringes of the lubrication film measured when the bubble starts to flow and when it is pushed to flow again after its first stop in the channel, respectively. (Scale bar, 100 μm.) (*C*) The derived film thickness and the contact length corresponding to the fringes in *B*, *i* and *ii*. (*D*) The measured driving pressure to overcome the friction resistance under the different contact length in the push-stop experiment, ~1 to 5 indicates 5 groups of repeated experiments.

Bretherton equation, $h \sim R \times Ca^{2/3}$, where h is the film thickness, Ca is the capillary number, $Ca = \mu U/\sigma$, μ is the fluid viscosity, σ is the surface tension of bubble in the blood, and U is the velocity of bubble. Flowing in a smaller channel, a bubble will have a thinner lubrication film, and thus, the clot will contact the wall in shorter time and the air embolism happens more easily. Actually, in clinical studies (20, 35, 36), the bubbles are more easily trapped in the smaller vessels after a bubble enters smaller branches and breaks into daughter bubbles. This phenomenon is also found in our experiment in vitro. The bubble flows through the first three levels, as shown in Fig. 2H, while most of them are trapped in the fourth level of the channels with the smallest size, as shown in Fig. 2I.

When the size of the vessel decreases to the scale of 10^1 μm, the Laplace pressure will take effect on the stopping of the bubble. In the capillaries within the size of tens of microns, the Laplace pressure is higher than the driven pressure, which will prevent the bubble from entering or flowing through the capillary. In clinical studies, small bubbles are often found to be blocked at the entrance of the capillaries (8, 16). On the other hand, when the vessel is larger than the bubble, the slug flow will not be formed. Therefore, the mechanism of the air embolism provided in this work cannot be applied under that condition. But, when the bubble enters the smaller branches downstream, they will form the slug flow, and the model can be used again.

Secondly, the shape of the vessel, such as the curvature or the bifurcation, also affects the formation of air embolism. The clot growing on the bubble surface is difficult to deform, and it will stop the bubble at the curved part of the vessel or at the junction of the vessels. For example, in Fig. 2D, the clot at the tail of the bubble cannot pass the curved part of the channel, so the bubble stops there. In Fig. 2I, bubbles stop mostly at the junction of the channels with the same size. This influence of the vessel shape is also found in the experiment in vivo, where air emboli are often found in the curve part and the junctions of the vessels (37, 38).

Materials and Methods

In Vivo Experiment. New Zealand rabbits (4 mo old) were purchased from laboratory animal research center of Tsinghua University. All the experiments were conducted in accordance with the Institute's Guide for the Care and Use of Laboratory Animals and were approved by the ethical committee of Tsinghua University (Approval No. AP#18-CHS1). The rabbit was anesthetized with 3% pentobarbital sodium (1 mL/kg) via the ear vein. The abdominal cavity of the rabbit was opened, and a part of the small intestine was placed under a microscope (Olympus IX83) with connection of relevant mesentery vascular network. Before the injection, the root mesenteric artery was clamped; meanwhile, the blood was added with Ca²⁺ and mixed with an air bubble within 15 s. Then, the 0.1-mL blood and air mixture was injected within 10 s, and the clamp was released to allow the blood to flow into the vascular network downstream. A small vessel with a diameter of about 100 μm in the downstream of the injection point was observed continuously. The observation location was far enough from the injection point to avoid any observable change in the size of the vessel during the whole injection process. The motion of the bubbles and the formation of the air embolism were observed in the vascular network under the microscope.

Blood Sample Treatment. For the in vivo experiments, the blood injected to the rabbit mesentery vessels was collected from the heart of the rabbit and reserved in a sodium citrate anticoagulant tube. Before the injection, 90 μL CaCl₂/MgCl₂ (0.83% wt: 0.33% wt) solution was added to 0.5 mL blood sample to revive the potential of blood coagulation. For the in vitro experiments, an extra process was performed to probe the fibrin in the blood before adding the CaCl₂/MgCl₂ solution. Six microlitres of fluorescent dyed fibrinogen (FluorTM 594, Alexa Co.) with a concentration of 0.1% wt was added to 0.5 mL blood, and then the blood was treated in a 37 °C water bath for 15 min.

To avoid the possibility that some clot was present when the bubble was injected, the treatment time was strictly limited to 25 s, which is far less than the average thrombosis time (39). Besides, the in vitro experimental results show that no visible fluorescence labeled fibrin are found in the blood after injection until thrombus starts to appear at the tail of the bubble.

We note that the pale thrombus, mainly comprising fibrins, platelets, and a small number of RBCs, generally forms in arteries where the flow rate is high, while the red thrombus, mainly comprising RBCs, fibrins, and a small number of platelets, is usually generated in the veins, where the flow rate is low (40). The flow parameters of the in vitro and in vivo experiments cover the range from venous condition to arterial condition (41), which may result in red thrombus or pale thrombus. However, as the vessel is partially blocked by the bubble, the velocity of the blood cells around the bubble are slowed down, and the clots formed in experiments both in vivo and in vitro are all found to be rich in RBCs and fibrins, which is more consistent with the red thrombus as shown in *SI Appendix*, Fig. S4. The labeled fibrin is used as an indicator of the positions and structure of thrombus around bubbles, and the platelets are also found in the thrombus, but their number is low (*SI Appendix*, Fig. S4).

Histological Section of Air Emboli. After the real-time observation on the air embolism found in the mesentery vascular network, the proximal and the distal ends of mesentery artery where the air embolism is located were ligated with 0# surgical suture, then cut off the artery and fixed in 4% paraformaldehyde for 24 h. Paroxydehyde acts on the functional group of amino acid side chain of protein polypeptide chain, forming a methylene bridge (-CH₂-) between protein polypeptide molecules, so that the structure of proteins will not change, antigenicity can be preserved and fine structure of tissue can be maintained, which are suitable for the preparation of tissue specimens and cell slices and long-term preservation. The fixed vascular tissue was embedded in paraffin and then sectioned and stained. All procedures were performed in strict accordance with the tissue section preparation specifications, in order to present the histological morphology of the observed phenomena. The histology sections were made along the sagittal plane in the center of the artery with the thickness of 10 μm. The bubble stuck in the vessels with the surrounding clot and was observed using a fluorescent microscope (Olympus IX83), as shown in Fig. 1 *D–F*.

Microfluidic Devices. The single serpentine PDMS channel and the channel network were made according to the soft photolithography method (27). BSA was coated on the inner wall of the channel by flowing 2% BSA solution in the channel for 1 h. Then air is infused into the channel to remove the extra BSA solution. To measure the flow field and the lubrication film around the bubble, round glass capillaries with the inner diameter of 300 μm are used to simulate the shape of the vessels. The BSA coating process is also applied to the glass capillaries. The prepared mixture of the dyed rabbit blood and air is injected into the glass capillary and the flow fields is then measured.

Measurement of the Flow Field around a Bubble. 100 μL reserved blood was centrifugated at the speed of $3000 \times g$ for 10 min and then rinsed with phosphate-buffered saline (1×, HyClone) for 3 times. The same buffer was added into the blood to adjust the RBCs concentration to 1% HCT for the flow field measurement. The choice of concentration is for clearer visualization of the flow field. The concentration difference from the whole blood will have influences on the positions of stagnant points, but the experiment is still valid to show the recirculation zones in front of and behind the moving bubble, which is consistent with the result in the experiment with whole blood shown in Movie S5. The blood sample was injected into the glass device with a flow rate of 1 mL/h, and the movement of the RBCs was captured by a high-speed camera (M100, Phantom Co.) with a frame rate of 400 fps. According to the captured motion of the cells around a flowing bubble, the flow field around a bubble was obtained using the software of the particle image velocimetry (DynamicStudio, Dantec Co.).

Conclusion

In this work, both in vivo and in vitro experiments are performed to illustrate how a bubble stops from its flowing status to form the air embolism in a small vessel. The experimental results show that when the bubble is still moving, the clot starts to form on the rear of the bubble and finally stops the bubble. During the braking process of the bubble, the coagulation on a bubble surface is found to play a dominant role in the formation of the air embolism, and it is greatly influenced by the flow fields around a bubble confined in the small vessel.

Attributed to the flow field around a bubble, the clot is found to originate at the tail of the bubble. The recirculation flow at the tail of the bubble brings cells and fibrinogens to the bubble surface, while the flow in front of the bubble pushes the cells and fibrinogens

Li et al.
Flow field around bubbles on formation of air embolism in small vessels

PNAS | 5 of 6
https://doi.org/10.1073/pnas.2025406118

away from the bubble. With the accumulation of cells and fibrinogens at the tail of the bubble, the fibrins and a few platelets are found around the bubble, and the clot forms.

As the clot on the bubble grows, it will gradually break the lubrication film between the bubble and the channel wall, which is illustrated using an optical interference method. The measured friction force on the bubble is found to increase rapidly as the clot contacts with more area of the channel wall, and the increased friction force will stop the motion of the bubble and cause the air embolism in the vessel.

Although the microfluidic channels still have some limitations in mimicking the in vivo situation, such as the lack of endothelial on the channel wall, the difference of elasticity between materials, etc., the phenomena that the flow recirculation induces thrombus formation and stops the bubble in the microvessel are consistent in the in vivo and in vitro experiments. This is strong evidence of the validity of the microfluidic chips to mimic the microvessels in this study. This work brings insight into the mechanism of air embolism

that the formation of the air emboli starts when a bubble is still in the flowing status. Under the flowing condition, the fluid dynamics of the slug flow and the lubrication play an important role in the formation of air embolism in small vessels, while the Laplace pressure of the bubble has much less influence than previously believed. This work helps us to better understand the mechanism of air embolism, and the microfluidic methods used in the in vitro experiment have potential applications in the drug research on embolization and thrombolysis.

Data Availability. All study data are included in the article and/or supporting information.

1. L. Bartolini, K. Burger, Pearls & oy-sters: Cerebral venous air embolism after central catheter removal: Too much air can kill. *Neurology* **84**, e94–e96 (2015).
2. C. M. Muth, E. S. Shank, Gas embolism. *N. Engl. J. Med.* **342**, 476–482 (2000).
3. N. Nerlekar *et al.*, Peripheral air embolism. *Lancet* **382**, 1070 (2013).
4. V. Papadopoulou, M. X. Tang, C. Balestra, R. J. Eckersley, T. D. Karapantsios, Circulatory bubble dynamics: From physical to biological aspects. *Adv. Colloid Interface Sci.* **206**, 239–249 (2014).
5. R. D. Vann, F. K. Butler, S. J. Mitchell, R. E. Moon, Decompression illness. *Lancet* **377**, 153–164 (2011).
6. D. Dennis, V. Secasanu, M. Conroy, J. Smith, J. McCallister, A hollow heart: A case of massive venous air embolism. *Chest* **156**, A2024 (2019).
7. R. M. Bass, D. B. Longmore, Cerebral damage during open heart surgery. *Nature* **222**, 30–33 (1969).
8. Y. Bernaldo de Quirós *et al.*, Bubbles quantified in vivo by ultrasound relates to amount of gas detected post-mortem in rabbits decompressed from high pressure. *Front. Physiol.* **7**, 310 (2016).
9. H. E. Roberts, S. A. Smith, Disorders of the respiratory system in pet and ornamental fish. *Vet Clin North Am Exot Anim Pract* **14**, 179–206 (2011).
10. C. J. McCarthy, S. Behravesh, S. G. Naidu, R. Oklu, Air embolism: Practical tips for prevention and treatment. *J. Clin. Med.* **5**, 93 (2016).
11. R. P. Weenink, M. W. Hollmann, R. A. van Hulst, Animal models of cerebral arterial gas embolism. *J. Neurosci. Methods* **205**, 233–245 (2012).
12. K. Lambrechts *et al.*, Venous gas emboli are involved in post-dive macro, but not microvascular dysfunction. *Eur. J. Appl. Physiol.* **117**, 335–344 (2017).
13. K. Zhang *et al.*, Time course of endothelial dysfunction induced by decompression bubbles in rats. *Front. Physiol.* **8**, 181 (2017).
14. F. P. Bretherton, The motion of long bubbles in tubes. *J. Fluid Mech.* **10**, 166–188 (1961).
15. G. I. Taylor, Deposition of a viscous fluid on the wall of a tube. *J. Fluid Mech.* **10**, 161–165 (1961).
16. J. L. Bull, Cardiovascular bubble dynamics. *Crit. Rev. Biomed. Eng.* **33**, 299–346 (2005).
17. J. E. Hall, *Guyton and Hall Textbook of Medical Physiology* (Saunders, Elsevier, ed. 12, 2011).
18. T. W. Beck, S. Daniels, D. M. Paton, E. B. Smith, Detection of bubbles in decompression sickness. *Nature* **276**, 173–174 (1978).
19. B. M. Blokker *et al.*, Conventional autopsy versus minimally invasive autopsy with postmortem MRI, CT, and CT-guided biopsy: Comparison of diagnostic performance. *Radiology* **289**, 658–667 (2018).
20. V. Papadopoulou *et al.*, Variability in circulating gas emboli after a same scuba diving exposure. *Eur. J. Appl. Physiol.* **118**, 1255–1264 (2018).
21. J. Fabre, A. Line, Modeling of two-phase slug flow. *Annu. Rev. Fluid Mech.* **24**, 21–46 (1992).
22. A. B. Branger, D. M. Eckmann, Theoretical and experimental intravascular gas embolism absorption dynamics. *J Appl Physiol (1985)* **87**, 1287–1295 (1999).
23. S. Samuel, A. Duprey, M. L. Fabiilli, J. L. Bull, J. B. Fowlkes, In vivo microscopy of targeted vessel occlusion employing acoustic droplet vaporization. *Microcirculation* **19**, 501–509 (2012).
24. A. J. Calderon *et al.*, Microfluidic model of bubble lodging in microvessel bifurcations. *Appl. Phys. Lett.* **89**, 244103 (2006).
25. D. M. Eckmann, S. L. Diamond, Surfactants attenuate gas embolism-induced thrombin production. *Anesthesiology* **100**, 77–84 (2004).
26. D. M. Eckmann, S. C. Armstead, F. Mardini, Surfactants reduce platelet-bubble and platelet-platelet binding induced by in vitro air embolism. *Anesthesiology* **103**, 1204–1210 (2005).
27. J. C. McDonald *et al.*, Fabrication of microfluidic systems in poly(dimethylsiloxane). *Electrophoresis* **21**, 27–40 (2000).
28. M. Kobari *et al.*, Blood flow velocity in the pial arteries of cats, with particular reference to the vessel diameter. *J. Cereb. Blood Flow Metab.* **4**, 110–114 (1984).
29. H. Lamport, Flowmeter design for continuous immediate measurement of red cell velocity-profile in microvessels. *Nature* **206**, 132–135 (1965).
30. Y. E. Yu, S. Khodaparast, H. A. Stone, Armoring confined bubbles in the flow of colloidal suspensions. *Soft Matter* **13**, 2857–2865 (2017).
31. K. J. Stebe, S. Y. Lin, C. Maldarelli, Remobilizing surfactant retarded fluid particle interfaces. I. Stress-free conditions at the interfaces of micellar solutions of surfactants with fast sorption kinetics. *Phys. Fluids A Fluid Dyn.* **3**, 3–20 (1991).
32. E. Yamaguchi, B. J. Smith, D. P. Gaver III, µ-PIV measurements of the ensemble flow fields surrounding a migrating semi-infinite bubble. *Exp. Fluids* **47**, 309–320 (2009).
33. R. Fåhræus, T. Lindqvist, The viscosity of the blood in narrow capillary tubes. *Am. J. Physiol.* **96**, 562–568 (1931).
34. J. D. Ruiter, R. Lagraauw, D. D. Ende, F. Mugele, Wettability-independent bouncing on flat surfaces mediated by thin air films. *Nat. Phys.* **11**, 48–53 (2015).
35. M. P. Spencer, Y. Oyama, Pulmonary capacity for dissipation of venous gas emboli. *Aerosp. Med.* **42**, 822–827 (1971).
36. B. D. Butler, B. A. Hills, The lung as a filter for microbubbles. *J. Appl. Physiol.* **47**, 537–543 (1979).
37. A. Prasad, S. Banerjee, E. S. Brilakis, Images in cardiovascular medicine. Hemodynamic consequences of massive coronary air embolism. *Circulation* **115**, e51–e53 (2007).
38. I. P. Torres Filho, L. N. Torres, B. D. Spiess, In vivo microvascular mosaics show air embolism reduction after perfluorocarbon emulsion treatment. *Microvasc. Res.* **84**, 390–394 (2012).
39. J. M. Siller-Matula, R. Plasenzotti, A. Spiel, P. Quehenberger, B. Jilma, Interspecies differences in coagulation profile. *Thromb. Haemost.* **100**, 397–404 (2008).
40. M. Koupenova, B. E. Kehrel, H. A. Corkrey, J. E. Freedman, Thrombosis and platelets: An update. *Eur. Heart J.* **38**, 785–791 (2017).
41. S. Singhal, R. Henderson, K. Horsfield, K. Harding, G. Cumming, Morphometry of the human pulmonary arterial tree. *Circ. Res.* **33**, 190–197 (1973).

6 of 6 | PNAS
https://doi.org/10.1073/pnas.2025406118

Li et al.
Flow field around bubbles on formation of air embolism in small vessels